Joint Shadowing Process in Urban Peer-to-Peer Radio Channels

Zhenyu Wang, Eustace K. Tameh, and Andrew R. Nix

***Abstract*—For multihop and *ad hoc* networks, a conventional 1-D channel model cannot capture the spatial correlation of the shadowing processes. This paper investigates the joint spatial correlation property of the shadowing process for peer-to-peer (P2P) radio links in urban environments. When a fixed base station is assumed, statistical analysis reveals that the shadowing process is mainly a result of spatial displacement at the mobile station (MS). Furthermore, the joint correlation property of the MS–MS channel shows that MS displacements at each end of the P2P link have an independent and equal effect on the correlation coefficient. A sum-of-sinusoids simulation model is proposed to generate the joint correlation shadowing process for urban P2P radio channels. The performance of the proposed channel simulator is analyzed in terms of the autocorrelation and joint correlation function of the simulated shadowing process. Simulations illustrate that the proposed model is able to output deterministic shadowing with a normal distribution (in decibels) and the desired correlation properties. It is thus suitable for use in system-level simulations, such as the evaluation of routing and radio resource management algorithms in *ad hoc* or mesh networks.**

***Index Terms*—Ad hoc, channel model, multihop, shadowing, spatial correlation, urban.**

I. Introduction

THE DEMAND for flexible mobile multimedia services continues to grow. Traditional cellular solutions are coming under increasing pressure from wireless peer-to-peer (P2P) systems such as *ad hoc* networks [1] and wireless local area networks (WLANs) [2] (IEEE 802.11a/b/g, and their outdoor extensions 802.11p/s). Beyond third-generation networks are looking to combine P2P connectivity, together with traditional cellular solutions to improve coverage, reduce transmit power, and ultimately provide ubiquitous high-capacity connectivity [3]–[6]. One of the core ideas in such networks is the provision of high-capacity connectivity through P2P links. These short-range connections avoid large shadowing losses and, thus, offer a more efficient spatial reuse of the radio resource [3], [4]. The need to evaluate the performance of routing protocols and radio resource management (RRM) schemes in such networks calls for channel models that properly reflect the cross-spatial-correlation properties of the shadowing process for meshed links between mobile nodes.

Most existing shadowing correlation models [7]–[11] are established based on the base station (BS)-to-mobile station (MS) propagation channel for cellular networks, where only the MS moves. In [12], the cross correlation of MS to multi-BS links was modeled for handoff performance analyses. The shadow fading between two BSs and two MSs was studied in [13]. However, in a multihop or *ad hoc* network, the shadowing correlation property over a large number of MS–MS links (where the MSs are free to move at both ends of the link) requires close investigation. In [14], it was reported that incomplete consideration of the spatial correlation in a multipoint-to-multipoint radio channel (i.e., multiple MS–MS links) can lead to significant simulation inaccuracies, particularly for routing protocol and RRM performance evaluation. In this paper, our first contribution investigates the joint spatial correlation property of the shadowing process for meshed P2P and *ad hoc* wireless links in a dense urban environment. The shadowing correlation for dual terminal mobility links is modeled using a joint correlation function (JCF). The analysis is based on channel data obtained from a detailed site-specific 3-D ray-tracing model. This model was previously developed and validated at the University of Bristol [16], [17].

In addition to the correlation model previously discussed, it is also necessary to develop an appropriate simulation model (presented in this paper) to generate correlated shadowing for system-level performance evaluation. In [13], a general mathematical joint correlation model with two BSs and two MSs was derived. In the 3GPP Spatial Channel Model [15], it is suggested that correlation between channels from one mobile to two BSs be introduced by multiplying random Gaussian variables with an appropriate correlation matrix. However, these approaches are impractical when applied to true P2P networks due to the large number of meshed channels between mobile nodes. In [15], the fast-fading correlation between antenna elements in a multi-input–multi-output channel was introduced by pregenerating a set of directional multipaths. Unfortunately, this method cannot be used for generating correlated shadowing unless we know and are able to model the spatial correlation properties of the scatterers seen by all radio nodes in the test area, which is far from trivial. In [14], it is suggested that a simple biased fading (random or site specific) process be applied to each MS; however, no detailed method is provided. We conclude that no efficient shadowing process models are

Manuscript received January 9, 2006; revised September 22, 2006 and December 11, 2006. This work was supported in part by the IST-2001-32549 ROMANTIK Project. The review of this paper was coordinated by Dr. K. Dandekar.

Z. Wang was with the Centre for Communications Research, University of Bristol, BS8 1TH Bristol U.K. He is now with IPWireless, SN15 1BN Wiltshire, U.K. (e-mail: jwang@ipwireless.com).

E. K. Tameh was with the Centre for Communications Research, University of Bristol, BS8 1TH Bristol U.K. He is now with ProVision Communication Technologies Ltd., BS4 4EU Bristol, U.K. (e-mail: eustace.tameh@provision-comm.com).

A. R. Nix is with the Centre for Communications Research, University of Bristol, BS8 1TH Bristol U.K. (e-mail: andy.nix@bris.ac.uk).

Digital Object Identifier 10.1109/TVT.2007.904513

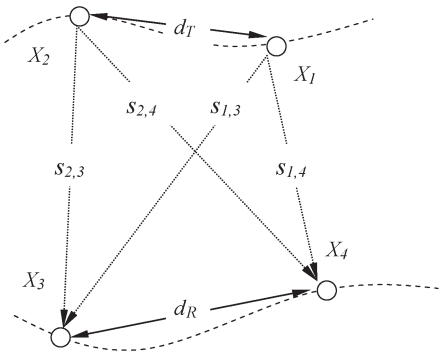

Fig. 1. *Ad hoc* system model.

currently available in the literature to support system-level P2P and *ad hoc* simulations.

In our second contribution, a sum-of-sinusoids (SOS) simulation model is proposed to generate the joint shadowing process in an urban P2P wireless network. The SOS method has been shown to have many advantages, particularly in terms of accuracy and speed for simulating fast-fading channels [19]–[22]. One example of this method is the popular Jake's simulation model for Rayleigh fading channels [26]. Recently, the SOS method has been used to simulate the 1-D shadowing process for a BS–MS radio link [20] and the 2-D shadowing process [11] that accommodates the situation where the MS moves along a closed route (i.e., a route with a common start and end point), rather than a straight line. In our paper, a discrete Monte Carlo sampling method (DMCM) is proposed to determine the spatial frequencies of the sinusoidal waveforms according to the spatial power spectrum, which is calculated from the JCF that was developed in the first part of this paper. The performance of the resulting channel simulator is analyzed in terms of the average squared error (ASE) of the corresponding JCF relative to the theoretical (and, hence, desired) JCF, the shadowing cumulative distribution function (cdf), and the simulation speed. Simulations are used to illustrate the potential of the newly proposed model.

The remainder of this paper is organized as follows: In Section II, the system model and assumptions are described. In Section III, the 3-D ray model used to obtain channel data is introduced, and the shadowing correlation property is analyzed. The proposed simulation model is presented in Section IV. An analysis of the proposed model is given in Section V together with a step-by-step implementation guide. A number of concluding remarks are drawn in Section VI.

II. System Model and Assumptions

Fig. 1 illustrates a physical model of an *ad hoc* network with meshed P2P links. We denote a radio node in the network by $X_i := (x_i, y_i)$, with x_i and y_i representing the physical location coordinate in a given test area. The radio nodes directly transmit to one another, with each node being capable of acting as a transmitter (Tx) or a receiver (Rx). The shadowing (shadow fading) fluctuation in radio link (i, j) is denoted by $s_{i,j}$, which is defined as the variance in the local path loss (averaged over tens of wavelengths) around the distance-dependent mean path loss (averaged over a large number of Tx and Rx locations in the same radio environment and at a given separation distance) [8], [24].

Assuming that the shadowing fluctuation is wide sense stationary, and $s_{i,j}$ can be characterized by its first- and second-order statistics, then from various experimental results, it has been shown [8], [23], [25] that the shadowing fluctuation can be characterized by a zero-mean normal distribution (in decibels). Hence, $s_{i,j}$ can be modeled as

$$s_{i,j}[dB] = N(0, \sigma_s) \tag{1}$$

where $N(0, \sigma_s)$ represents a normal distribution with zero mean $(\mu = 0)$ and standard deviation σ_s. For a conventional cellular network, the spatial correlation of the shadowing fluctuation is characterized by an autocorrelation function (ACF) for the MS-to-a-single-static-BS (BS–MS) link [7]–[11] and by a cross-correlation function (CCF) for the MS-to-multiple-static-BSs link [12], [13].

For an *ad hoc* network, it is assumed that all nodes have the same configuration (e.g., antenna type and height) and that they communicate to one another through a common channel. Hence, the shadowing fluctuations seen by the nodes at both ends of the radio link are identical, i.e., $s_{i,j} = s_{j,i}$. This is very different compared to a conventional cellular network, where the radio link is established between different types of equipment, e.g., a BS at 15 m above ground level (AGL) and an MS at 1.5 m AGL. Interchanging the BS and MS locations in a cellular system results in different shadowing fluctuations, i.e., $s_{i,j} \neq s_{j,i}$ (note that interchanging the subscripts here implies the physical swapping of Tx and Rx locations). Based on the aforementioned assumptions, the standard deviation of $s_{i,j}$ can be estimated using

$$\sigma_s^2 = E\left\{s_{i,j}^2\right\}_{i,j} = E\left\{s_{j,i}^2\right\}_{j,i} \tag{2}$$

where $E\{\cdot\}_{i,j}$ represents the expectation operator over all possible nodes pair X_i and X_j. The CCF between the shadowing fluctuation in the two links (e.g., $s_{1,3}$ and $s_{2,4}$ in Fig. 1) has the same form as the ACF for a single link when the nodes at both ends move (e.g., one end moves from X_1 to X_2, while the other moves from X_3 to X_4). To distinguish between the ACF and CCF used for cellular networks in previous literature, the correlation function of the shadowing fluctuation in an *ad hoc* network is referred to here as a JCF.

Finally, as in prior literature [7]–[13], we assume that the spatial correlation function of the shadowing fluctuation is only a function of the distance moved by the nodes (i.e., their position shifts). More specifically, the correlation is said to be statistically isotropic (i.e., on average, the same in all directions). Hence, the JCF (i.e., R_s) can be expressed as

$$R_s(\mathbf{d}_T, \mathbf{d}_R) = E\{s_{i,j} \cdot s_{i',j'}\}/\sigma_s^2 \tag{3}$$

where $\mathbf{d}_T$ and $\mathbf{d}_R$ represent the displacement of the transmitter and receiver, respectively, i.e., $\mathbf{d}_T = |X_i - X_{i'}|$ and $\mathbf{d}_R = |X_j - X_{j'}|$.

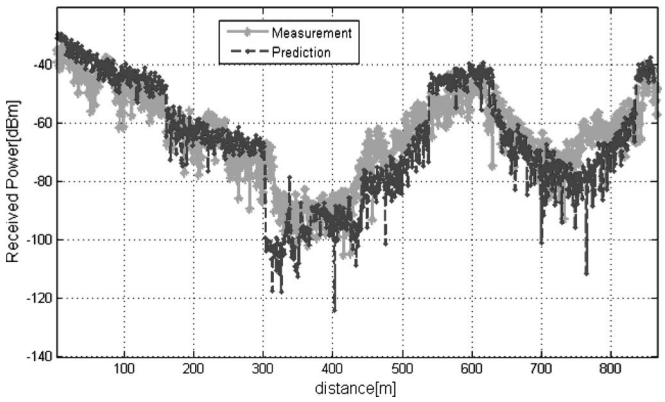

Fig. 2. Example of urban validation for the ray model: Low-mounted BS (3 m). The mean error is −2.5 dB, and the RMSE is 6.8 dB.

III. Shadowing Correlation Property

To characterize the shadowing fluctuation correlation in a P2P network accurately, it is necessary to obtain channel data between all the meshed links in the network. It is extremely difficult (as well as impractical) to obtain sufficient channel data samples by means of measurement alone. To overcome this limitation, a fully 3-D deterministic propagation model [16] has been used to generate the significant sets of propagation data that are required to statistically analyze the shadowing processes. The model uses geographic data (terrain, building, foliage, and ground cover data) to predict power as well as time, frequency, and spatial dispersion in the radio channel. The model was developed at the University of Bristol over a period from 1996 to 2004 and has been validated for cellular (and microcellular) applications, where the Tx is located above (and well below) the rooftop level at frequencies of 2 and 5 GHz [16], [17]. Fig. 2 provides an example of the model's validation (performed in the center of Bristol) [17]. The data were collected at 1.8 GHz using a 3-m-high Tx dipole antenna and a 1.5-m-high Rx dipole antenna. The mean error in the predicted received power level (compared to the measured one) was −2.5 dB, with an RMSE of 6.8 dB. The predicted power level was found to be highly correlated (0.94) with the measured data; hence, the prediction error on a point-by-point basis has an insignificant impact on the evaluation of the correlation of the shadowing process.

In our previous study of the P2P radio channel [23], we found that the shadowing fluctuation of P2P links can be well modeled as a Gaussian process (normal distribution). In this section, we focus on the correlation properties of the shadowing process.

A. Ray Model Simulations

Simulations are based on an area of central Bristol. This urban environment is representative of a European city with typical three-storey building heights. The average building height and road width for this region is 12 m (including pitched roofs) and 20 m, respectively. Vertical dipole antennas were assumed at the Tx and Rx. Three-dimensional antenna field patterns were incorporated in the model, and features such as polarization are included in the power and path loss predictions. The impact of the human body and the effects of moving objects (such as vehicles) were not included in the analysis. The simulations were performed at frequencies of 2.1 and 5.2 GHz.

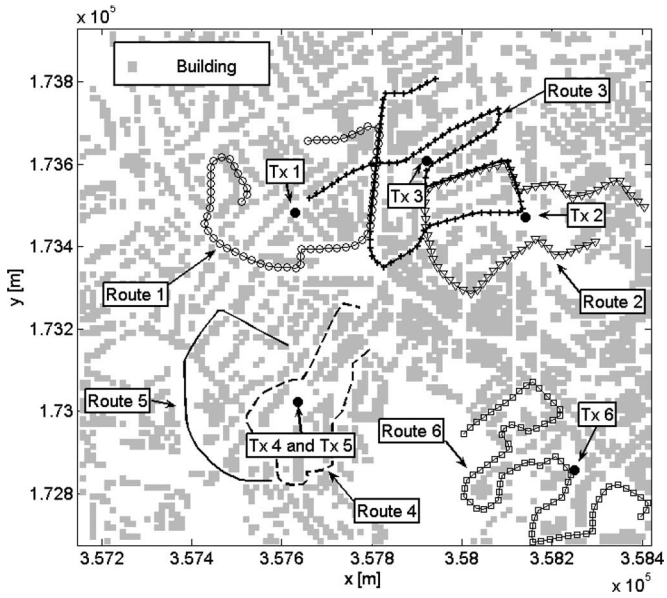

Fig. 3. Route settings for single terminal mobility scenario.

To study the spatial correlation of the channel in the case where only one end of a link moves, six routes were defined as shown in Fig. 3. The simulations were performed with a fixed Tx location and with the Rx moving along each of the defined routes (this is referred to as a "single terminal mobility" scenario, to differentiate it from the case where terminals at both ends of the radio link are mobile). As the spatial correlation is environment dependent, to obtain the average correlation function, the six routes were placed in different areas of the map, with a total length of 8 km. The Tx/Rx were located at 1.5 m AGL to simulate mobile radio terminals (MS units). To compare with the well-known shadowing fluctuation correlation property in a cellular network, the Tx height was varied to simulate a WLAN access point (AP) at 5 m AGL and a microcellular BS at 15 m AGL.

To study the P2P JCF (where terminals at both ends of the link are free to move), a pair of routes was defined for each simulation, with one route representing Tx movement and the other representing Rx movement (this is referred to as a "dual terminal mobility" scenario). Four route pairs were defined in the central area of the city, with a total length of 2 km for the Tx and 2 km for the Rx. The route pairs are shown in Fig. 4. The Tx and Rx terminals were set to a height of 1.5 m AGL. In both simulation scenarios, channel data were generated with the Rx (and the Tx in the dual terminal mobility scenario) moving along the preset routes at 1-m intervals. The shadowing fluctuation data were calculated by subtracting the predicted local path loss (where the effects of fast fading were removed using suitable averaging) from the distance-dependent mean path loss found in our previous P2P radio channel study [23].

B. Spatial ACF

The spatial correlation property of the shadowing fluctuation in a single link, where only one end is free to move, can be

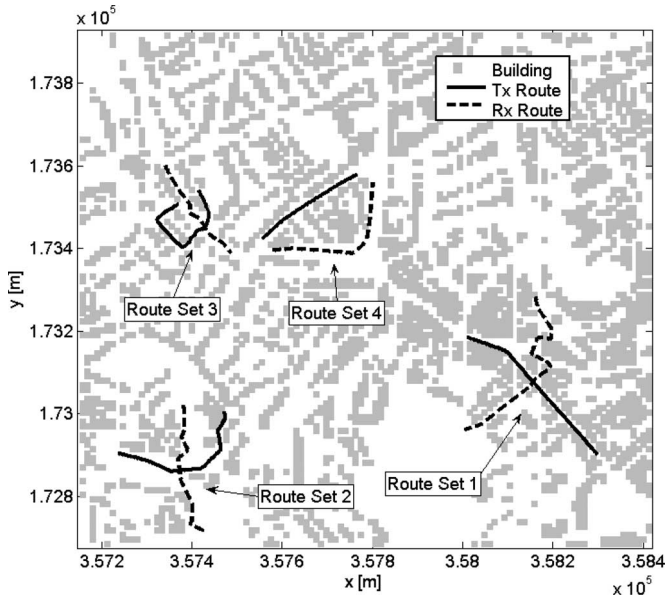

Fig. 4. Route settings for dual terminal mobility scenario.

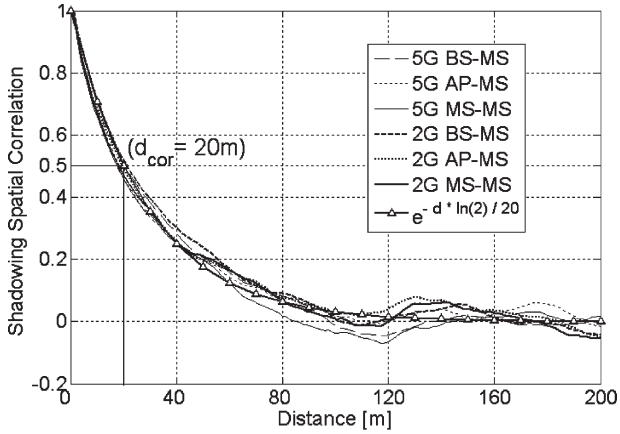

Fig. 5. ACF from single terminal mobility scenario simulations.

characterized by its ACF. From previous experiments reported in the literature [9], [10], it was found that the spatial ACF of the shadow fading process can be modeled using an exponential decay function, which is represented by

$$R_1(\mathbf{d}_R) = R_s(0, \mathbf{d}_R) = \exp\left(-\frac{|\mathbf{d}_R|}{d_{\text{cor}}} \ln 2\right) \tag{4}$$

where $\mathbf{d}_R$ represents the movement of the Rx, and d_{cor} represents the decorrelation distance. The value of d_{cor} depends on the environment and corresponds to the distance at which the correlation drops to 0.5.

In this paper, the ACF is estimated by feeding the channel data from the single terminal mobility scenario into (3), where parameter $\mathbf{d}_T$ is set to zero (i.e., only the Rx is free to move). Since we assume that the shadowing fluctuation seen in the downlink is identical to that in the uplink for a P2P channel, the ACF for a moving Tx and a fixed Rx (i.e., $\mathbf{d}_R = 0$) will have the same form (as confirmed later in Fig. 7). The ACF has been calculated for each of the six routes described in Section III-B. These data have been averaged and are plotted in Fig. 5. It can be observed from the figure that the estimated ACF curves agree well with the exponential decay function. For the city of Bristol, the best fit (least squares fitting) decorrelation distance d_{cor} for MS–MS links was found to be approximately 20 m (19.6 m at 5 GHz and 20.2 m at 2 GHz) with RMSEs of less than 0.002.

Furthermore, it can be seen from Fig. 5 that the ACFs for a wide range of link types (BS–MS, AP–MS, and MS–MS) are similar, not withstanding the varying Tx heights and operating frequencies. This is reasonable since the shadowing fluctuation is actually a result of the birth and death of multipaths, which correspond to the changing scatterers in the vicinity of the Tx and Rx. During the simulations, only the Rx, i.e., the MS, is allowed to move, and hence, the shadowing fluctuation is mainly caused by the changing environment (i.e., buildings) surrounding the MS. It should be noted that differences in the distance-dependent mean path loss between different channel types have already been removed during the calculation of the shadowing fluctuation, and hence, this is not seen in the correlation properties. Furthermore, the standard deviation of the shadowing fluctuation (which is studied in [23]) does not have any impact on the resulting correlation value.

C. Joint Spatial Correlation Function

The spatial correlation property of the shadowing fluctuation in a radio link where both ends are in motion (or between two different links) is characterized by the JCF. The JCF is estimated by feeding the channel data from the dual terminal mobility scenario into (3). Fig. 6 shows the averaged spatial JCF for the shadowing fluctuation, where the Tx and Rx displacements ($\mathbf{d}_T$ and $\mathbf{d}_R$) are limited to 100 m. For shifts beyond 100 m, the correlation coefficient was found to lie between 0.1 and -0.1.

Fig. 7 shows two slice planes through Fig. 6, for $\mathbf{d}_T = 0$ and $\mathbf{d}_R = 0$, respectively, i.e., functions $R_s(0, \mathbf{d}_R)$ and $R_s(\mathbf{d}_T, 0)$, which correspond to cases where only the Rx or Tx moves. As expected, the two curves are very close to the exponential decay ACF extracted previously from the single terminal mobility simulations, with mean absolute errors of 0.045 and 0.048, and RMSEs of 0.052 and 0.054 for $R_s(0, \mathbf{d}_R)$ and $R_s(\mathbf{d}_T, 0)$, respectively (within the distance interval [0 m, 100 m]).

Fig. 6(b) shows a contour plot of the JCF. It can be seen that, when the correlation coefficient is greater than 0.2, the contour lines are approximately straight and lie at an angle of 45°. This indicates that the movements of the Tx and Rx have an independent and equal impact on the value of the JCF. Assuming that the shadowing fluctuation is only a result of changes in the local scatterers around the moving terminals and that the terminal movements are uncorrelated at both ends of the link, the JCF can be approximated by the product of the two ACF functions, as follows:

$$\begin{aligned} R_s(\mathbf{d}_T, \mathbf{d}_R) &= R_s(\mathbf{d}_T, 0) \cdot R_s(0, \mathbf{d}_R) \\ &= \exp\left(-\frac{|\mathbf{d}_T| + |\mathbf{d}_R|}{d_{\text{cor}}} \ln 2\right). \end{aligned} \tag{5}$$

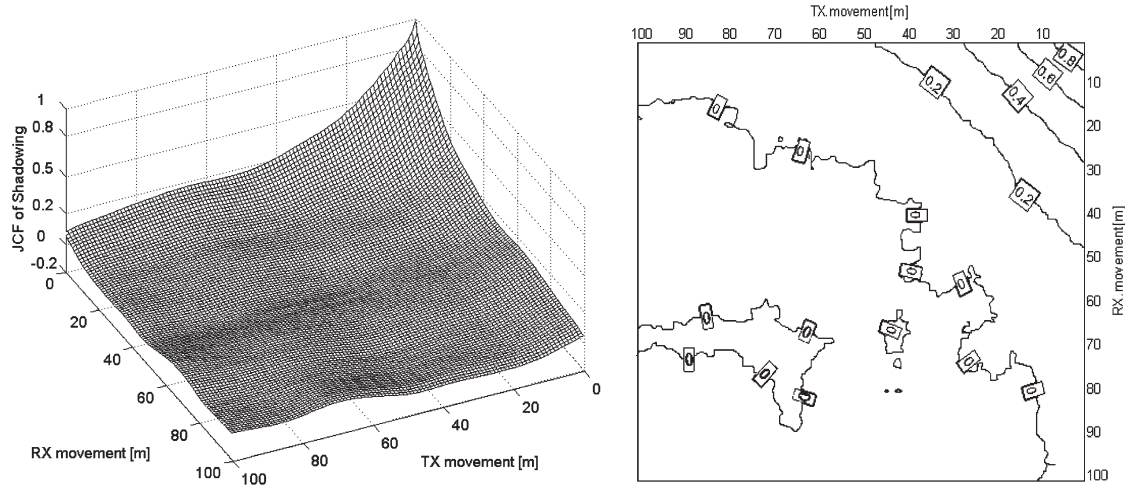

Fig. 6. JCF from dual terminal mobility scenario simulations. (a) 3-D plot and (b) contour plot.

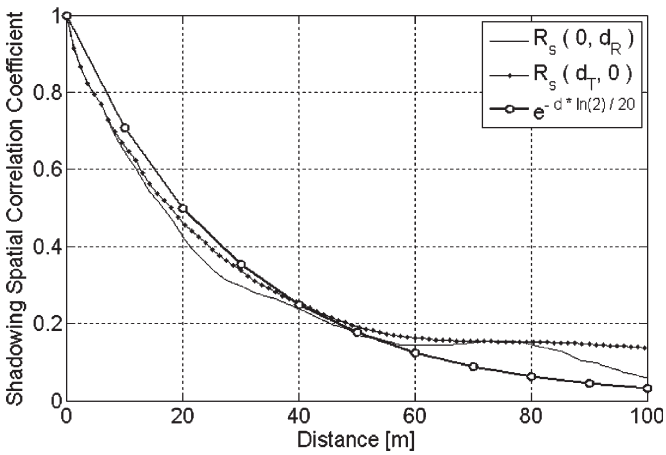

Fig. 7. Comparison between ACF and slices of the JCF.

Using this approximation, the mean absolute error and the RMSE between $R_s(\mathbf{d}_T, \mathbf{d}_R)$ and $R_s(\mathbf{d}_T, 0)R_s(0, \mathbf{d}_R)$ are 0.028 and 0.037, respectively, for $\mathbf{d}_T$, $\mathbf{d}_R \leq 100$ m).

IV. Simulation Model

As previously mentioned, it is essential to accurately regenerate the joint shadow fading process in P2P wireless communications. In the literature, several design methodologies have been reported to simulate the fading channel. The vast majority of these methods can be classified into one of three categories.

1) The SOS method, which is based on the fact that a Gaussian random process can be expressed as an infinite SOS with random phases and properly selected frequencies [18]. In practice, a finite number of sinusoids can be used to approximate the Gaussian process, and this is used to reduce complexity [19]. This method is frequently used to simulate correlated fast-fading processes (e.g., [19] and [26]) and has been used more recently to model shadowing processes [11], [20].
2) The filter-based method, where channel data are generated by means of low-pass filtering a zero-mean white Gaussian noise process (e.g., [27] and [28]). The underlying principle is that a stationary Gaussian process can be generated by passing a sequence of white Gaussian random deviates through a filter whose frequency response is the square root of the Gaussian process's power spectral density (PSD) [29, p. 403].
3) Channel design methods based on Markov processes. This method is often used (e.g., [31] and [32]) to model radio link properties, such as the *signal-to-noise ratio* and the *bit error rate*, instead of using physical propagation characteristics.

The SOS approach has been shown to have considerable advantages in terms of accuracy and speed [19]–[22]. The statistical properties of SOS-based channel simulation models are presented in [21]. A fast implementation scheme based on a lookup table is recommended in [22]. The SOS method is studied in some detail in [19], with four different techniques developed to compute the coefficients of the simulation model.

In this section, a SOS-based simulation model is proposed for the joint shadowing processes seen in urban P2P radio channels. A DMCM is used to determine the spatial frequencies of the sinusoidal waveforms based on the spatial power spectrum, which is calculated from the JCF of the P2P shadowing process.

A. SOS Simulation Model

The simulation model for a Gaussian random process $s(t)$ based on the SOS method described in [19] can be expressed as a 1-D function in time, i.e.,

$$\hat{s}(t) = \sum_{n=1}^{N} c_n \cos(2\pi f_n t + \theta_n) \tag{6}$$

where $\hat{s}(t)$ is the approximate version of $s(t)$, and N represents the number of sinusoids. Strictly speaking, when N is finite,

the stochastic process $\hat{s}(t)$ is non-Gaussian. Nevertheless, the cdf of $\hat{s}(t)$ will be close to a Gaussian process if N is sufficiently large, e.g., in the range of 6–30 according to [19]. $\{\theta_n\}_{n=1}^N$ represent sets of uniformly distributed random phase variables in the range $[0, 2\pi)$. $\{f_n\}_{n=1}^N$ and $\{c_n\}_{n=1}^N$ represent the frequency set and the corresponding amplitude coefficient set, respectively, which are determined such that the resulting $\hat{s}(t)$ has an identical (or as close as possible) PSD to that of $s(t)$. The PSD of Gaussian random process $s(t)$ can be calculated by performing the Fourier transform of the ACF of $s(t)$ [18].

As previously mentioned, the shadowing fluctuation can be modeled using a Gaussian random process as a function of the Tx and Rx locations. Here, $s(x, y, u, v)$ is used to represent the shadowing fluctuation, with $[x, y]$ and $[u, v]$ indicating the Tx and Rx positions in the test area, respectively. $s(x, y, u, v)$ can also be presented as a function of time $s(t)$, in cases where the Tx and Rx are in motion. The displacements of Rx and Tx are represented as $\mathbf{d}_T := [\Delta x, \Delta y]^T$ and $\mathbf{d}_R := [\Delta u, \Delta v]^T$, respectively (where $[\cdot]^T$ represents the transpose operation). Equation (6) is now extended to a 4-D spatial Gaussian process to simulate the spatially correlated shadowing process for a P2P radio channel

$$\begin{aligned}\hat{s}(x, y, u, v) &= \sum_{n=1}^{N} c_n \cos\left(2\pi \mathbf{f}_n [x, y, u, v]^T + \theta_n\right) \\ &= \sum_{n=1}^{N} c_n \cos\left[2\pi (f_{x,n} x + f_{y,n} y + f_{u,n} u \right. \\ &\qquad \left. + f_{v,n} v) + \theta_n\right] \end{aligned} \tag{7}$$

where $\hat{s}(x, y, u, v)$ determines the shadowing fluctuation value on a virtual map characterized by the spatial frequency set $\{\mathbf{f}_n\}$, the corresponding coefficients $\{c_n\}$, and phases $\{\theta_n\}$. The discrete spatial frequencies $\mathbf{f}_n := [f_{x,n}, f_{y,n}, f_{u,n}, f_{v,n}]$ represent four element vectors. We further define spatial frequencies $\mathbf{f}_{T,n} := [f_{x,n}, f_{y,n}]$ and $\mathbf{f}_{R,n} := [f_{u,n}, f_{v,n}]$; and continuous frequency variables $\mathbf{f}_T := [f_x, f_y]$, $\mathbf{f}_R := [f_u, f_v]$, and $\mathbf{f} := [f_x, f_y, f_u, f_v]$.

The ACF in (4) is extended to a 2-D function as follows:

$$R_1(\mathbf{d}_T) = \exp\left(-\frac{|\mathbf{d}_T|}{d_{\text{cor}}} \ln 2\right) = \exp\left(-\frac{\sqrt{\Delta x^2 + \Delta y^2}}{d_{\text{cor}}} \ln 2\right) \tag{8}$$

(for the case where only the Tx moves, which is also identical to the case where only the Rx moves). The JCF in (5) is also extended to a 4-D function as

$$R_2(\mathbf{d}_T, \mathbf{d}_R) = R_1(\mathbf{d}_T) \cdot R_1(\mathbf{d}_R). \tag{9}$$

The spatial frequency set $\{\mathbf{f}_n\}$ and the coefficients $\{c_n\}$ for $\hat{s}(x, y, u, v)$ in (7) can be determined by sampling the 4-D PSD of the Gaussian random process $s(x, y, u, v)$. To obtain the desired PSD, we need to perform a Fourier transform on the 4-D ACF (i.e., the JCF, as explained in Section II) of $s(x, y, u, v)$ in (9). This gives

$$\begin{aligned}\Phi_2(\mathbf{f}) &= \int_{-\infty}^{\infty}\int_{-\infty}^{\infty} R_2(\mathbf{d}_T, \mathbf{d}_R) \\ &\quad \cdot e^{-j(2\pi \mathbf{f}_T \cdot \mathbf{d}_T + 2\pi \mathbf{f}_R \cdot \mathbf{d}_R)} d(\mathbf{d}_T) d(\mathbf{d}_R) \\ &= \int_{-\infty}^{\infty} R_1(\mathbf{d}_T) \cdot e^{-j \cdot 2\pi \mathbf{f}_T \cdot \mathbf{d}_T} d(\mathbf{d}_T) \int_{-\infty}^{\infty} R_1(\mathbf{d}_R) \\ &\quad \cdot e^{-j \cdot 2\pi \mathbf{f}_R \cdot \mathbf{d}_R} d(\mathbf{d}_R) \\ &= \Phi_1(\mathbf{f}_T) \cdot \Phi_1(\mathbf{f}_R) \end{aligned} \tag{10}$$

where $\Phi_2(\mathbf{f})$ represents the 4-D PSD of $s(x, y, u, v)$, and $\Phi_1(\mathbf{f})$ is the Fourier transform of the correlation function $R_1(d)$ in (8). The following expression gives the closed-form solution of $\Phi_1(\mathbf{f}_T)$ (and an equivalent process gives $\Phi_1(\mathbf{f}_R)$), as derived in [11], where $a = \ln(2)/d_{\text{cor}}$:

$$\Phi_1(\mathbf{f}_T) = \frac{2\pi a}{\left[a^2 + 4\pi^2 |\mathbf{f}_T|^2\right]^{\frac{3}{2}}} = \frac{2\pi a}{\left[a^2 + 4\pi^2 \left(f_x^2 + f_y^2\right)\right]^{\frac{3}{2}}}. \tag{11}$$

There are four methods proposed in [19] to sample the desired PSD to determine the spatial frequency set $\{\mathbf{f}_n\}$ and the coefficients $\{c_n\}$ in a SOS model. These methods have been previously used to model shadowing processes in [11] and [20].

1) the uniform sampling method (USM, also known as the equal distance method);
2) the nonuniform sampling method (NUSM, also known as the equal areas method);
3) the Monte Carlo method (MCM);
4) the mean-squared error method (MSEM). (In [20], the author uses a general form, L_P-norm method, with order $p = 2$).

From the first three methods, it is found in [11] that the MCM, with frequency set $\{\mathbf{f}_n\}$ generated according to a given *probability density function* (pdf) (which in turn is determined by the PSD), gives the best performance in terms of the ASE of the correlation functions of the simulated shadowing process (the mathematical definition can be found in Section IV-C) versus the number of sinusoids N. However, this method has the highest computational complexity. The USM method, where the PSD is uniformly sampled with frequency spacing $2\Delta f$ and $C_n^2/2$ represents the power of the PSD in the frequency interval $[f_n - \Delta f, f_n - \Delta f)$, requires a large number of sinusoids but has two useful features:

1) The result $\hat{s}(\cdot)$ is a periodical function, which is desirable when the user wants to wrap the shadowing fluctuation values around the simulated radio environment to avoid interference edge effects, and/or to simulate a large network.
2) It can be implemented using a lookup table on a computer or in hardware (which is fast).

It will be shown later in the analyses of the models that a large number of sinusoids are required to reduce the ASE of a

4-D JCF, even when the MCM method is used; hence, a high-speed simulation scheme is necessary. In the remainder of this section, the proposed DMCM is described, which is a combination of the MCM and USM. Following this, a number of performance evaluations are discussed. The MSEM presented in [19] and [20] does not have a closed-form solution and is therefore not considered further in this paper.

B. DMCM

In a pure MCM, the 4-D spatial frequency set $\{\mathbf{f}_n\}$ in (7) can be generated according to a given joint pdf, which is related to the PSD of the joint shadowing process. More specifically, the sampling frequencies can be generated according to a pdf that is proportional to the PSD [32]. From (8), it is straightforward to decompose the joint pdf for $\mathbf{f}$ into two independent and identical pdfs for $\mathbf{f}_T$ and $\mathbf{f}_R$, as shown in

$$p_2(\mathbf{f}) = b_2\Phi_2(\mathbf{f}) = b_2\Phi_1(\mathbf{f}_T)\Phi_1(\mathbf{f}_R) = b_1 p_1(\mathbf{f}_T)p_1(\mathbf{f}_R) \quad (12)$$

where $p_1(\cdot)$ and $p_2(\cdot)$ denote the 2-D pdf and 4-D joint pdf, respectively, and b_1 and b_2 are constants used to ensure that the integration of the pdf is equal to unity. Therefore, $\mathbf{f}_{T,n}$ and $\mathbf{f}_{R,n}$ can be generated independently. $p_1(\cdot)$ and the functions that were used to generate $\mathbf{f}_{T,n}$ (and $\mathbf{f}_{R,n}$ since it has an identical pdf) have been derived in [11]

$$|\mathbf{f}_T| = \frac{a}{2\pi}\sqrt{\frac{1}{(1-\beta)^2}} - 1,$$

$$f_x = |\mathbf{f}_T|\cos(\varphi), \qquad f_y = |\mathbf{f}_T|\sin(\varphi) \quad (13)$$

$$\theta_n = U(0, 2\pi) \quad (14)$$

where β is a random variable uniformly distributed over the range [0, 1], and φ is uniformly distributed over $[0, 2\pi)$. θ_n in (7) is a random variable uniformly distributed over $[0, 2\pi)$ and can be expressed using (14). The coefficients $\{c_n\}$ have the same value for all sinusoids [19] and are defined by the total power of the Gaussian random process s.

To enable an efficient implementation of the MCM, an equivalent discrete realization of (7) is introduced, which is known as the DMCM. First, the frequency sampling interval is defined to be $2\Delta f$, as in the USM method. The original sinusoid $\mathbf{f}_n$ is then modified from the pure MCM according to

$$\bar{f}_{x,n} = \text{round}\left[\frac{f_{x,n} + \Delta f}{2\Delta f}\right] \cdot 2\Delta f - \Delta f = (2m_{x,n} + 1)\Delta f \quad (15)$$

where $m_{x,n}$ is an integer. $\bar{f}_{y,n}$, $\bar{f}_{u,n}$, and $\bar{f}_{v,n}$ are modified in the manner previously described by (15). This modification forces the resulting Gaussian random process to have a period of $1/\Delta f$. Next, we set $\Delta\theta = 2\pi/N_{\text{Table}}$ to represent the resolution of the stored sinusoidal waveform, with the table size denoted by N_{Table}. $\{\theta_n\}$ is now modified as

$$\bar{\theta}_n = \text{round}\left(\frac{\theta_n - \Delta\theta/2}{\Delta\theta}\right) \times \Delta\theta = l_n\Delta\theta \quad (16)$$

where $l_n \in \{0, 1, \ldots, N_{\text{Table}} - 1\}$. Finally, the spatial sampling interval is set to $\Delta x = 1/(N_{\text{Table}}\Delta f)$, and $[\bar{x}, \bar{y}, \bar{u}, \bar{v}] = [k_x, k_y, k_u, k_v] \cdot \Delta x, k. \in \mathbb{Z}$. Equation (7) can now be rewritten in a discrete form as

$$\bar{s}(\bar{x}, \bar{y}, \bar{u}, \bar{v}) = \sqrt{\frac{N}{2}}\sum_{n=1}^{N}\cos\left\{\frac{2\pi}{N_{\text{Table}}}\Big[(2m_{x,n}+1)k_x + (2m_{y,n}+1)k_y + (2m_{u,n}+1)k_u + (2m_{v,n}+1)k_v + l_n\Big]\right\} \quad (17)$$

where $\bar{s} = (\bar{x}, \bar{y}, \bar{u}, \bar{v})$ represents a discrete Gaussian random process. It is easy to see from (17) that, when $N_{\text{Table}} \to \infty$, the DMCM becomes a pure MCM when $\Delta f \to \infty$ or a pure USM when $N \to \infty$. As all the elements in the operator $\sum$ are in the set $\{\cos(2\pi \cdot i/N_{\text{Table}})\}$, $i \in \{0, 1, \ldots, N_{\text{Table}} - 1\}$, (17) can be implemented on a computer using a lookup table, with all operations involving integers; hence, the simulation speed is high. According to [22], (17) can be realized in a multiplier-free hardware simulator; however, this falls outside the scope of this paper.

In P2P networks, all nodes normally communicate to one another through a common channel, and hence, the shadowing fluctuation in the uplink and downlink is expected to be identical, i.e., $s(x, y, u, v) = s(u, v, x, y)$. To account for this fact, the symmetric DMCM is introduced. Letting N be even, we first generate the first half of the frequency set $\{\mathbf{f}_n\}(n = 1, 2, \ldots, N/2)$, as previously described. The second half of this set is then generated using

$$\mathbf{f}_{n+N/2} = \mathbf{f}_n \cdot \begin{bmatrix} 0 & \mathbf{I} \\ \mathbf{I} & 0 \end{bmatrix}, \qquad \mathbf{I} = \begin{bmatrix} 1 & 0 \\ 0 & 1 \end{bmatrix}; n = 1, 2, \ldots, N/2 \quad (18)$$

$$\theta_{n+N/2} = \theta_n, \qquad n = 1, 2, \ldots, N/2 \quad (19)$$

i.e., $\mathbf{f}_{T,n} = \mathbf{f}_{R,n+N/2}$ and $\mathbf{f}_{R,n} = \mathbf{f}_{T,n+N/2}$, where $n = 1, 2, \ldots, N/2$. It should be noted that $\mathbf{f}_{T,n}$ and $\mathbf{f}_{R,n}$ are still independently generated. The preceding modification makes the discrete spatial frequency set $\{\mathbf{f}_n\}$ symmetric with respect to (w.r.t.) $\mathbf{f}_T = \mathbf{f}_R$, which results in symmetric shadowing fluctuation values for the uplink and downlink. This does not change the shape of the 4-D joint pdf since the pdf is symmetric in the same manner (i.e., w.r.t. $\mathbf{f}_T = \mathbf{f}_R$,). We also let $\theta_n = \theta_{n+N/2}(n = 1, 2, \ldots, N/2)$. This modification prevents the phase set $\{\theta_n\}$ from containing purely random values and thus introduces additional and unwanted correlations between $\mathbf{f}_n$ and $\mathbf{f}_{n+N/2}$. Therefore, some degree of degradation is expected for the DMCM when symmetric properties (symmetric DMCM) are required (compared to a nonsymmetric DMCM). This degradation is analyzed in Section V.

C. Performance Metrics

Three performance metrics are proposed to evaluate the Gaussian random process simulator: 1) the cdf of the output

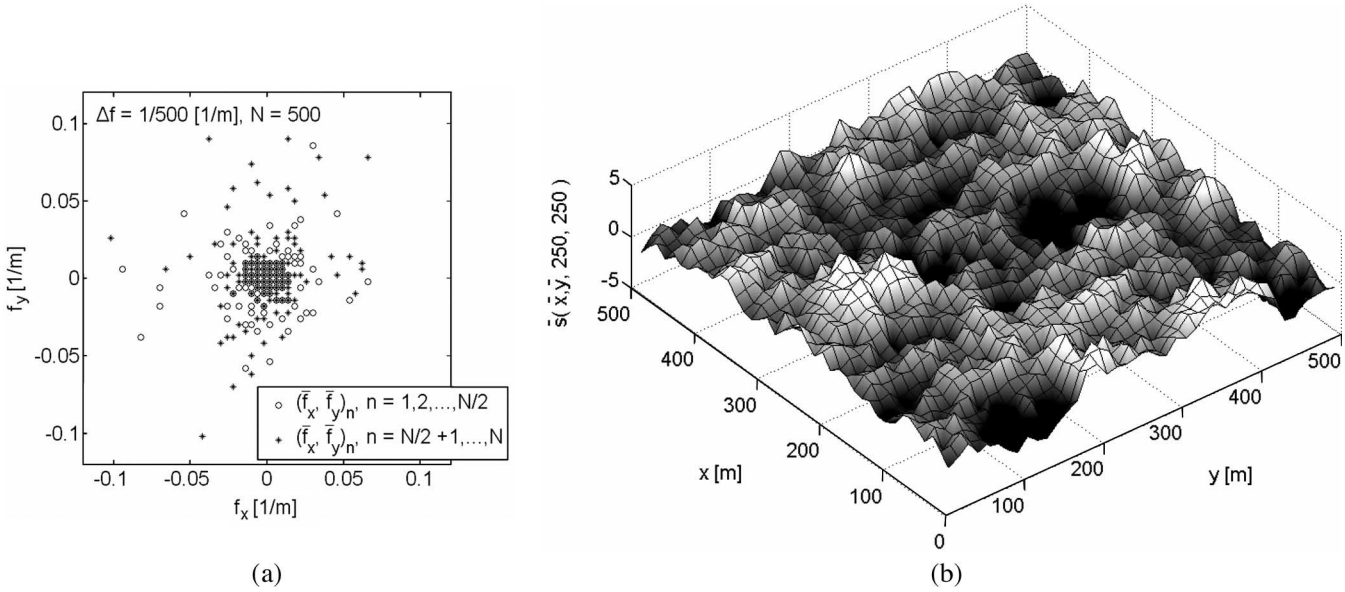

Fig. 8. Realization of the DMCM method. (a) Sample frequencies and (b) sample of the shadowing process.

values (i.e., the shadowing fluctuation); 2) the simulation speed; and 3) the ASE of the resulting correlation function.

The ASE of the correlation function was introduced in [11] and is defined as the ASE between the correlation functions of the simulated process $\hat{s}(\cdot)$ and the desired correlation functions of the shadowing process. It is equal to the square of the root-mean-square error (RMSE).

For the USM, MCM, and nonsymmetric DMCM, given that the only random variables in (7) are $\{\theta_n\}$, the JCF (i.e., the 4-D spatial ACF) of $\hat{s}(x, y, u, v)$ can be evaluated using the following expression:

$$\begin{aligned} &R_{\hat{s}}(\Delta x, \Delta y, \Delta u, \Delta v) \\ &= E\left\{\hat{s}(x, y, u, v)\hat{s}(x+\Delta x, y+\Delta y, u+\Delta u, v+\Delta v)^*\right\} \\ &= \sum_{n=1}^{N} \frac{c_n^2}{2} \cos\left[2\pi(f_{x,n}\Delta x + f_{y,n}\Delta y + f_{u,n}\Delta u + f_{v,n}\Delta v)\right] \end{aligned} \tag{20}$$

where $(\cdot)^*$ denotes the complex conjugate.

For the symmetric DMCM, (20) is no longer valid due to the introduction of symmetry in the phase set $\{\theta_n\}$, and $R_{\hat{s}}(\cdot)$ must be directly evaluated from the generated data.

The ASE of the JCF (ASE) can be evaluated using (21) via numerical integration. Since the Gaussian random process that was generated using the USM and symmetric DMCM is periodic, only the ASE in the range $[-1/(4\Delta f), 1/(4\Delta f)]$ has to be evaluated for these methods. Letting $X = Y = U = V = 1/(2\Delta f)$, since the JCF is symmetric w.r.t. $X = Y (U = V)$, the following equation can be written:

$$\begin{aligned} \text{ASE} = \frac{1}{XYUV} \int_{-X/2}^{X/2} \int_{-Y/2}^{Y/2} \int_{-U/2}^{U/2} \int_{-V/2}^{V/2} &\left[R_{\hat{s}}(\Delta x, \Delta y, \Delta u, \Delta v)\right. \\ &\left. - R_2(\Delta x, \Delta y, \Delta u, \Delta v)\right]^2 d\Delta x d\Delta y d\Delta u d\Delta v. \end{aligned} \tag{21}$$

V. Model Implementation and Numerical Result

In the following section, a range of numerical results are presented using the DMCM channel simulation model. The performance of the proposed model with different parameter settings is studied and compared against the pure MCM and USM in terms of the ASE of the JCF, the cdf of the output values, and the simulation speed. A step-by-step implementation guide is also given, together with suggestions on the parameter settings.

A. Numerical Results

The proposed model can be used to generate a virtual shadowing map with the desired correlation properties. As the SOS method gives deterministic output, the virtual map is stored in terms of a set of sinusoids at each considered point, instead of the actual shadowing fluctuation values. The shadowing fluctuation for any Tx–Rx link within this virtual map is then calculated on demand. This enables the model to implement the shadowing process over a large geographic region without the need for excessive memory space. A step-by-step implementation guide for the proposed model can be found in Section V-C.

Fig. 8 shows a realization of the SOS model using the symmetric DMCM. The decorrelation distance, the number of discrete 4-D spatial sinusoids, and the lowest frequency are set to 20 m (from Section III-A), $N = 500$, and $\Delta f = 1/500$ m, respectively. Hence, the period of the output shadowing process is 500 m. The sinusoid waveform table size is set to 200. As the discrete frequency set $\{\bar{\mathbf{f}}_n\}$ is symmetric w.r.t. $\mathbf{f}_T = \mathbf{f}_R$, only $\bar{\mathbf{f}}_{T,n}$ is plotted in the figure. The output sample is generated by defining a number of Tx positions over a 500 m $\times$ 500 m grid with 2-m spacing and fixing the Rx to lie at a location at the center of the test area (single terminal mobility study).

The 2-D ACF is evaluated using the data from the single terminal mobility studies and is plotted in Fig. 9, together

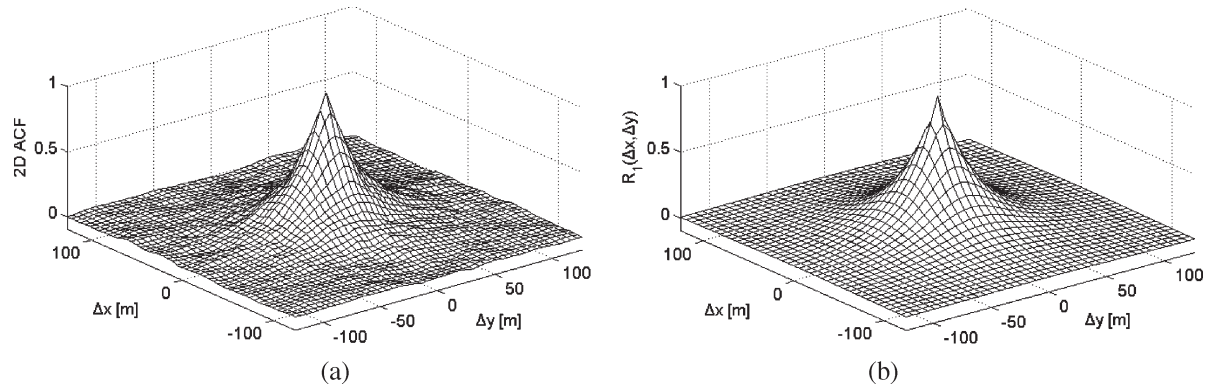

Fig. 9. Comparison of the evaluated and theoretical 2-D ACF. (a) Evaluated 2-D ACF and (b) theoretical 2-D ACF.

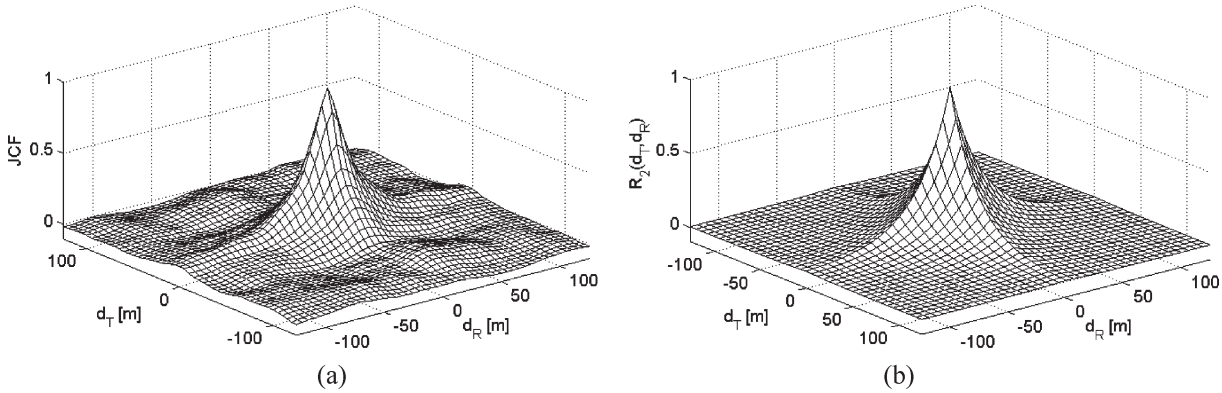

Fig. 10. Comparison of the evaluated and theoretical JCF. (a) Evaluated JCF and (b) theoretical JCF.

with the theoretical ACF. To evaluate the JCF, the shadowing fluctuation data are generated from a route analysis, where both the Tx and Rx move along two straight paths (dual terminal mobility study). The start points and the direction of motion for the Tx and Rx are random and independent. Fig. 10 shows the evaluated JCF, which is averaged over ten dual terminal mobility studies on one arbitrary DMCM realization.

B. Performance Analyses

Figs. 11 and 12 illustrate the ASE level for the JCF. Without loss of generality, the spatial scale is normalized by the decorrelation distance, i.e., $d_{\rm cor} = 1$. The number of spatial sinusoids N is varied in the range of 100–2000, Δf is varied from 1/6 to 1/40, and table size $N_{\rm Table}$ is varied from 200 to 1000. For the symmetric DMCM, $R_{\hat{s}}(\cdot)$ is evaluated directly from the generated data for single and dual terminal mobility studies. The resultant ASE is averaged over 30 realizations for each method.

It can be seen from Fig. 11 that the USM has better ASE performance compared to the other methods when Δf is less than 1/15. However, this performance is gained at the cost of an increased number of sinusoids as Δf decreases. For instance, for $\Delta f = 1/20$ and a 30-dB cutoff spatial frequency of $f_c = 1.1\ {\rm m}^{-1}$ (at which point the amplitude of the PSD in (11) is 30 dB lower than the amplitude at zero frequency), the number of sinusoids is $22^4/2$ for the 4-D process using USM; with the

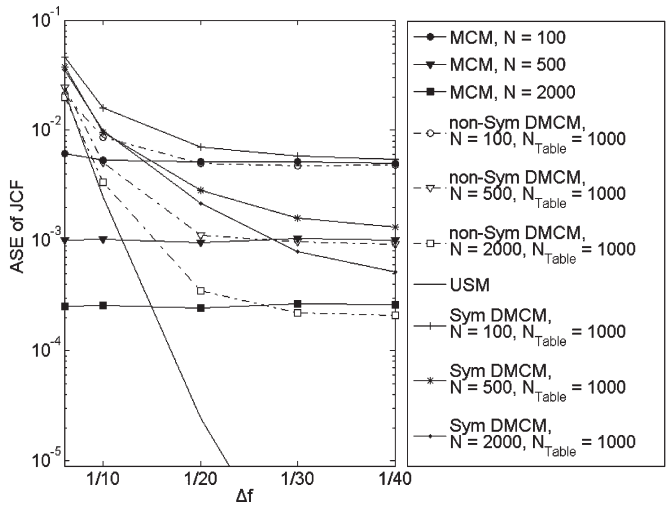

Fig. 11. ASE level of JCF.

number of sinusoids $N = 2048$ (i.e., $\Delta f = 1/6$), the ASE of the USM is only 0.02, which is worse than that of the other methods. The MCM offers the best performance compared to the symmetric and nonsymmetric DMCM with the same number of sinusoids N. The ASE improves from 10^{-2} to 10^{-3} as the number of sinusoids is increased from 100 to 500 for both the 2-D ACF and JCF.

The ASE performance of the nonsymmetric DMCM is bounded by both the MCM and USM performance. This is

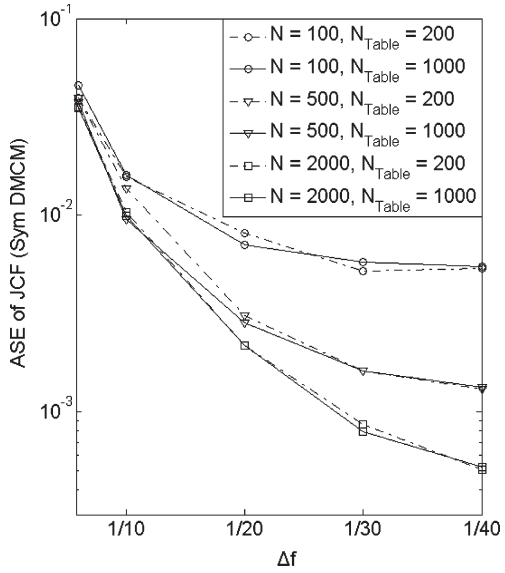

Fig. 12. Impact of N_{Table} on the ASE level of the JCF (symmetric, DMCM).

expected since the DMCM is a combination of these schemes. When Δf is greater than 1/10, the ASE level is high, and little performance gain is achieved by increasing the number of sinusoids N. This indicates that the performance degradation is mainly due to the large frequency sampling interval. As Δf increases, the ASE level of the DMCM drops and finally reaches the ASE level of the MCM with the same number of sinusoids. For N less than 500, a nonsymmetric DMCM can achieve a similar performance to the MCM when Δf reduces to 1/20, whereas, for N greater than 500, a smaller Δf value is required. In Fig. 12, it is seen that the reduction of table size N_{Table} from 1000 to 200 is seen to have little effect on the ASE level. However, in a real implementation of the shadowing model, the table size should not be too small since it is inversely proportional to the spatial sampling interval Δx, which itself must be much less than the decorrelation distance, i.e., the shadowing fluctuation at two adjacent sampling positions must be highly correlated.

Compared to the nonsymmetric DMCM, for the same parameter settings, the symmetric DMCM is seen to generate a higher ASE. To force symmetry, additional constraints were imposed on the phase of the sinusoids (see Section IV-B). This introduced additional correlation between frequencies sets $\bar{\mathbf{f}}_n$ and $\bar{\mathbf{f}}_{n+N/2}$ and, thus, a higher observed ASE. However, it can be seen from Fig. 12 that the degradation in performance can be reduced by increasing the frequency resolution $1/\Delta f$. For example, with the number of sinusoids $N = 100$, the ASE level of the symmetric DMCM becomes very close to that of the nonsymmetric DMCM when Δf decreases to less than 1/30.

Fig. 13 presents the cdf of the output values from the MCM and DMCM, both evaluated using 10^4 output samples from a single arbitrary realization for each method with random Tx and Rx positions. The results show that $N = 200$ is adequate to approximate a Gaussian process. There is a slight degradation in the cdf performance by increasing Δf from 1/50 to 1/10.

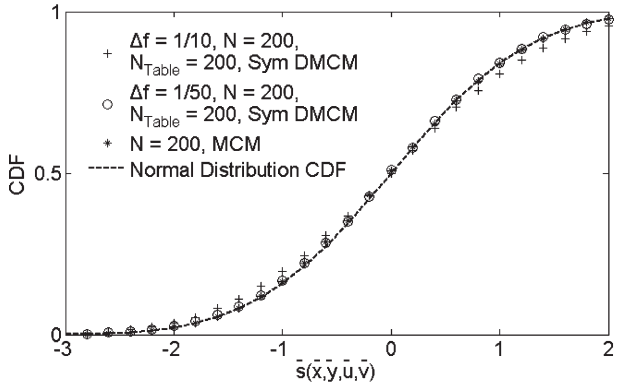

Fig. 13. CDF of the normalized shadowing value.

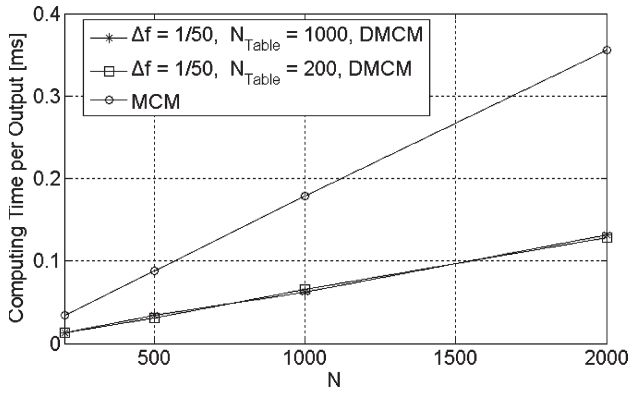

Fig. 14. Comparison of simulation speeds.

Fig. 14 shows the evaluated iteration time (time required to compute each output sample) for the pure MCM and DMCM. These data were obtained by averaging results over 10^5 output samples. To obtain a fair comparison between the speed of the different methods, the implemented code was written and compiled using the C programming language (using the standard math library), and all computing times are based on a 1.8-GHz Pentium IV processor running Windows XP. As only integer operations are involved in (15), the DMCM is seen to have a speed improvement over the pure MCM. The improvement factor is about 2.8, which is independent of the sinusoid number N, the table size N_{Table}, and Δf. With the sinusoid number N set to be less than 800, the DMCM can generate more than 20 000 output/s, which is sufficient for shadowing fluctuation processes in system-level simulations.

In summary, the MCM approach gives the best performance in terms of ASE versus the number of sinusoids used. The ASE level of the proposed DMCM model is bounded by the USM bound when the frequency sampling resolution is low (i.e., Δf is large). The DMCM can achieve the same ASE performance as the MCM when Δf decreases to a certain threshold. The value of this threshold depends on the number of sinusoids N in the model. Introducing symmetry (which is vital for P2P simulations) degrades the DMCM ASE performance significantly, particularly when Δf is large. However, a desired ASE level of, for example, $10^{-2.6}$ (corresponding to a mean absolute error of 0.05) can still be achieved by reducing Δf and/or increasing N.

C. Model Implementation

As many of the parameters for the DMCM are related and some of them have significant impact on model performance, the following step-by-step guide is given to aid in the implementation of the joint shadowing process model in mesh P2P networks in urban environments.

Step 1) Determine the parameters of the simulated radio environment, which include the following:
- the dimension of the virtual shadowing fluctuation map: x_{MAX} and y_{MAX}(i.e., the extent of the simulated region);
- the shadowing fluctuation parameters: standard deviation σ_s and decorrelation distance d_{cor}.

Step 2) Determine the parameters of the DMCM, which include the following:
- The number of sinusoids N: This should be great enough to ensure model accuracy. It should be noted that the model accuracy is also a function of Δf. According to the performance analyses in the previous section, for $\Delta f = d_{\mathrm{cor}}/20$, $N = 500$ is suggested.
- Frequency resolution Δf: This parameter defines the shadowing process periodicity. Therefore, $1/\Delta f$ must be no less than $\max[x_{\mathrm{MAX}}, y_{\mathrm{MAX}}]$. For increasing model accuracy, Δf should be as small as possible. However, decreasing Δf increases the size of the sinusoidal waveform table N_{Table}, i.e., it requires more computer memory, particularly when the spatial resolution Δx is set to a very small value. Decreasing Δf also results in larger periodicity, which is undesirable if a user wants to wrap a small virtual shadowing map to simulate large networks with many radio nodes (to reduce the network simulation time). $\Delta f < 1/(20 d_{\mathrm{cor}})$ is suggested.
- Spatial resolution Δx: The DMCM model is only able to directly generate the shadowing fluctuation on spatial grids with resolution Δx. For any Tx/Rx location off those grid points, the shadowing fluctuation value has to be spatially interpolated from the values at nearby grid points. The simplest (also the fastest) interpolating method is approximating the shadowing fluctuation by returning the value for the nearest grid point, in which case, Δx must be much less than the distance up to which the mean received power (and, hence, the shadowing fluctuation value) remains approximately constant. An accepted empirical bound is terminal movement over a few tens of wavelengths [8].
- The table size of the stored sinusoidal waveform is calculated by $N_{\mathrm{Table}} = 1/(\Delta x \cdot \Delta f)$.
- The suggested parameters are summarized in Table I.

TABLE I
PARAMETER GUIDELINES

Parameter	Symbol	Suggested Value
Shadowing Standard deviation	σ_s	8 -12 dB [8], or Advanced P2P link shadowing model [23]
de-correlation distance	d_{cor}	20m for typical European city
Number of sinusoids	N	$N = 500$
Frequency resolution	Δf	$\Delta f < 1 / (20\ d_{cor})$, and the map periodicity $1/\Delta f > \mathrm{MAX}(x_{MAX}, y_{MAX})$
Spatial resolution	Δx	$\Delta x < 10$ wavelengths
Waveform table size	N_{Table}	$N_{Table} = 1 / (\Delta x \cdot \Delta f)$

Step 3) Generate the random 4-D spatial continuous frequency set $\{\mathbf{f}_n\}$ and the phase set $\{\theta_n\}$ using (13) and (14), respectively. For the symmetric DMCM, only the first half of each set needs to be generated, with the second half calculated using (17) and (19). The coefficients c_n are set to be $\sqrt{2/N}$ for all sinusoids to generate a unity power Gaussian random process (i.e., $\sum c_n^2/2 = 1$).

Step 4) Transform the continuous frequency set $\{\mathbf{f}_n\}$ and the phase set $\{\theta_n\}$ into discrete forms using (15) and (16), respectively.

Having completed the preceding four steps, the virtual shadowing fluctuation map can then be determined. To generate a different shadowing fluctuation map for the same radio scenario, Steps 3) and 4) can be repeated. The shadowing fluctuation value between any pair of radio nodes on the virtual map can be calculated using Step 5).

Step 5) Calculate the unity power Gaussian value by inputting the Tx and Rx locations (after being transformed into their discrete forms using Δx) into (17). This value is then multiplied by the shadowing fluctuation standard deviation σ_s to obtain the exact shadowing fluctuation.

The physical location of each node can be set manually or can be randomly generated using a mobility model [33]. It is worth emphasizing that the DMCM method generates a periodic map, and the radio nodes can be considered to lie on the surface of a toroid.

VI. CONCLUSION

In this paper, the spatial correlation of the shadowing fluctuation for P2P radio links has been investigated, and its correlation functions have been extracted. Statistical analysis revealed that the shadowing fluctuation process is mainly a result of MS movement when a fixed BS is assumed. Its ACF in a single mobility scenario is well modeled by an exponential decay function, with a decorrelation distance of 20 m (for the city of

Bristol). Furthermore, the joint correlation property of a P2P link in a dual mobility scenario showed that MS movement at each end of the link has an independent and equal effect on the correlation coefficient. The JCF can be approximated by the product of two ACF functions in a single mobility scenario.

A novel simulation model for the joint shadowing processes in urban P2P radio channels was proposed. The underlying principle is that a Gaussian random process with a given PSD can be modeled as a SOS. The spatial frequencies of the sinusoidal waveforms were determined using DMCM. It generates periodic output, which wraps the simulated radio environment, and enables users to simulate large networks without fear of interference edge effects. In addition, this method can also be efficiently implemented on a computer (or hardware platform) by using lookup table techniques, which improve the simulation speed. Simulations illustrated that the proposed model is capable of generating shadowing fluctuation output values that approximate the Gaussian distribution (in decibels) and, with the desired correlation property, improves the accuracy/speed performance compared to other considered methods. In conclusion, the proposed model enables extensive system-level simulations of large P2P urban radio networks to be performed with correlated shadowing.

REFERENCES

[1] R. Ramanathan and J. Redi, "A brief overview of ad hoc networks: Challenges and directions," *IEEE Commun. Mag.*, vol. 40, no. 5, pp. 20–22, May 2002.

[2] A. Doufexi *et al.*, "A comparison of the HIPERLAN/2 and IEEE 802.11a wireless LAN standards," *IEEE Commun. Mag.*, vol. 40, no. 5, pp. 172–180, May 2002.

[3] *Opportunity Driven Multiple Access*, Dec. 1999. 3GPP TR 25.924 V1.0.0. 3GPP TSG-RAN.

[4] J. Vidal *et al.*, "Multi-hop networks for capacity and coverage enhancement in TDD/UTRAN," in *Proc. 1st Annu. Med-Hoc-Net*, Sardinia, Italy, Sep. 2002, pp. 234–239.

[5] A. N. Zadeh *et al.*, "Self-organizing packet radio ad hoc networks with overlay (SOPRANO)," *IEEE Commun. Mag.*, vol. 40, no. 6, pp. 149–157, Jun. 2002.

[6] M. Lott *et al.*, "Medium access and radio resource management for ad hoc networks based on UTRA TDD," in *Proc. ACM MobiHOC*, Long Beach, CA, Oct. 2001, pp. 76–86.

[7] "Digital mobile radio towards future generation systems, COST 231 Final Report," ISBN 92-828-5416-7, ch. 2 and 4, European Communities, 1999.

[8] L. M. Correia, *Wireless Flexible Personalized Communications, COST 259: European Co-Operation in Mobile Radio Research*, pp. 77–222, 2001.

[9] M. Gudmundson, "Correlation model for shadow fading in mobile radio systems," *Electron. Lett.*, vol. 27, no. 23, pp. 2145–2146, Nov. 1991.

[10] A. Gehring, M. Steinbauer, I. Gaspard, and M. Grigat, "Empirical channel stationarity in urban environments," in *Proc. 4th EPMCC*, Feb. 2001.

[11] X. Cai and G. B. Giannakis, "A two-dimensional channel simulation model for shadowing processes," *IEEE Trans. Veh. Technol.*, vol. 52, no. 6, pp. 1558–1567, Nov. 2003.

[12] H. Kim and Y. Han, "Enhanced correlated shadowing generation in channel simulation," *IEEE Commun. Lett.*, vol. 6, no. 7, pp. 279–281, Jul. 2002.

[13] F. Graziosi and F. Santucci, "A general correlation model for shadow fading in mobile radio systems," *IEEE Commun. Lett.*, vol. 6, no. 3, pp. 101–104, Mar. 2002.

[14] N. Patwari, Y. Wang, and R. J. O'Dea, "The importance of the multipoint-to-multipoint indoor radio channel in ad hoc networks," in *Proc. IEEE WCNC*, Mar. 2002, pp. 608–612.

[15] *Spatial Channel Model Text Description v7.0, 3GPP2*, (2003, Aug.). [Online]. Available: ftp://ftp.3gpp2.org/TSGC/Working/2003/3GPP_3GPP2_SCM

[16] E. K. Tameh and A. R. Nix, "A 3-D integrated macro and microcellular propagation model, based on the use of photogrammetric terrain and building data," in *Proc. 47th IEEE VTC*, May 1997, vol. 3, pp. 1957–1961.

[17] E. K. Tameh and A. R. Nix, "A mixed-cell propagation model for interference prediction in a UMTS network," in *Proc. 53rd IEEE VTC—Spring*, May 2001, vol. 1, pp. 409–413.

[18] S. O. Rice, "Mathematical analysis of random noise," *Bell Syst. Tech. J.*, vol. 23, pp. 282–332, Jul. 1944.

[19] M. Pätzold, U. Killat, and F. Laue, "A deterministic digital simulation model for Suzuki processes with application to a shadowed Rayleigh land mobile radio channel," *IEEE Trans. Veh. Technol.*, vol. 45, no. 2, pp. 318–331, May 1996.

[20] M. Pätzold and V. D. Nguyen, "A spatial simulation model for shadow fading processes in mobile radio channels," in *Proc. 15th IEEE PIMRC*, Sep. 2004, vol. 3, pp. 1832–1838.

[21] M. Patzöld, U. Killat, F. Laue, and Y. Li, "On the statistical properties of deterministic simulation models for mobile fading channels," *IEEE Trans. Veh. Technol.*, vol. 47, no. 1, pp. 254–269, Feb. 1998.

[22] M. Patzöld, R. García, and F. Laue, "Design of high-speed simulation models for mobile fading channels by using table look-up techniques," *IEEE Trans. Veh. Technol.*, vol. 49, no. 4, pp. 1178–1190, Jul. 2000.

[23] Z. Wang, E. K. Tameh, and A. R. Nix, "Statistical peer-to-peer channel models for outdoor urban environment at 2 GHz and 5 GHz," in *Proc. 60th IEEE VTC—Fall*, Sep. 2004, vol. 7, pp. 5101–5105.

[24] B. Sklar, "Rayleigh fading channels in mobile digital communication systems—Part 1: Characterization," *IEEE Commun. Mag.*, vol. 35, no. 7, pp. 90–100, Jul. 1997.

[25] W. C. Y. Lee, *Mobile Communications Engineering*. New York: McGraw-Hill, 1997.

[26] W. C. Jakes, *Microwave Mobile Communications*. Piscataway, NJ: IEEE Press, 1994.

[27] E. Lutz and E. Plöchinger, "Generating Rice processes with given spectral properties," *IEEE Trans. Veh. Technol.*, vol. VT-34, no. 4, pp. 178–181, Nov. 1985.

[28] S. A. Fechtel, "A novel approach to modeling and efficient simulation of frequency-selective fading radio channels," *IEEE J. Sel. Areas Commun.*, vol. 11, no. 3, pp. 422–431, Apr. 1993.

[29] A. Papoulis and S. Pillai, *Probability, Random Variables and Stochastic Processes*, 4th ed. New York: McGraw-Hill, 1973.

[30] H. S. Wang and N. Moayeri, "Finite-state Markov channel—A useful model for radio communication channels," *IEEE Trans. Veh. Technol.*, vol. 44, no. 1, pp. 163–171, Feb. 1995.

[31] C. Iskander and P. T. Mathiopoulos, "Fast simulation of diversity Nakagami fading channels using finite-state Markov models," *IEEE Trans. Broadcast.*, vol. 49, no. 3, pp. 269–277, Sep. 2003.

[32] P. Höeher, "A statistical discrete-time model for the WSSUS multipath channel," *IEEE Trans. Veh. Technol.*, vol. 41, no. 4, pp. 461–468, Nov. 1992.

[33] T. Camp, J. Boleng, and V. Davies, "A survey of mobility models for ad hoc network research," *Wireless Commun. Mobile Comput.—Special Issue Mobile Ad Hoc Networking: Research, Trends, Applications*, vol. 2, no. 5, pp. 483–502, Aug. 2002.

Zhenyu Wang received the B.Sc. degree in telecommunications from Xidian University, Xi'an, China, in 1997 and the M.Sc. and Ph.D. degrees in electrical and electronic engineering from the University of Bristol, Bristol, U.K., in 2001 and 2007, respectively.

From 1997 to 1999, he was with the Design Institute, Ministry of Post and Telecommunications, Zhengzhou, China, where he was involved in the design and optimization of GSM networks. In 2006, he joined Provision Communications Ltd., Bristol, where his work focused on the physical-layer optimization of WiMAX networks. In 2007, he moved to IPWireless, Wiltshire, U.K., where he is currently working on 3GPP-LTE system designs. His current research interests include channel modeling, radio planning, and optimization for multihop networks.

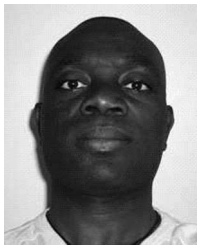

Eustace K. Tameh received the B.Sc. degree (with honors) in electronic engineering and mathematics from Keele University, Staffordshire, U.K., in 1994 and the Ph.D. degree in wide area propagation prediction and planning from the University of Bristol, Bristol, U.K., in 1998.

In 1997, he was a Research Associate with the University of Bristol, where he worked on research projects on propagation modeling and cellular network designs. In 2006, he joined ProVision Communication Technologies Ltd., Bristol, where he currently leads the development of RF planning tools. His current research interests include the development of novel planning techniques for broadband systems and multisystem integration for third-generation-and-beyond networks.

Andrew R. Nix received the B.Eng. and Ph.D. degrees from the University of Bristol, Bristol, U.K., in 1989 and 1993, respectively.

He then joined the Centre for Communications Research, University of Bristol, where he was a Member of Lecturing Staff and is currently a Professor of wireless communication systems. He has managed numerous projects that were funded by the European Union, the Engineering and Physical Sciences Research Council, and the Department of Trade and Industry. He has published more than 300 journal papers and conference proceedings. His main research interests include broadband wireless communications, radio-wave-propagation modeling, cellular-network optimization, and advanced digital modulation/reception techniques.